



OPEN ACCESS

EDITED BY
Estanislao Pujades,
Spanish National Research Council (CSIC),
Spain

REVIEWED BY
Mengjie Shi,
Liaoning Technical University, China
Yong Qian,
Chinese Academy of Geological Sciences
(CAGS), China
Qianzhu Zhang,
Changjiang River Scientific Research Institute
(CRSRI), China

*CORRESPONDENCE
Lyu Xiaoxi

☑ karstlv@gznu.edu.cn
Jiao Shulin
☑ jiaoshulin@gznu.edu.cn

RECEIVED 28 August 2025 ACCEPTED 31 October 2025 PUBLISHED 20 November 2025

CITATION

Jinglin M, Xiaoxi L, Shulin J, Jianghu H, Dongnan W, Chenyi Z, Chenpeng H and Renkai Z (2025) Hydrogeochemistry and water quality assessment in two dolomite karst springs: a case study from the Shibing dolomite karst, Guizhou plateau. Front. Water 7:1694469. doi: 10.3389/frwa.2025.1694469

COPYRIGHT

© 2025 Jinglin, Xiaoxi, Shulin, Jianghu, Dongnan, Chenyi, Chenpeng and Renkai. This is an open-access article distributed under the terms of the Creative Commons Attribution License (CC BY). The use, distribution or reproduction in other forums is permitted, provided the original author(s) and the copyright owner(s) are credited and that the original publication in this journal is cited, in accordance with accepted academic practice. No use, distribution or reproduction is permitted which does not comply with these terms.

Hydrogeochemistry and water quality assessment in two dolomite karst springs: a case study from the Shibing dolomite karst, Guizhou plateau

Mo Jinglin¹, Lyu Xiaoxi^{1,2,3}*, Jiao Shulin¹*, He Jianghu¹, Wang Dongnan^{1,2}, Zhu Chenyi^{1,2}, Hu Chenpeng⁴ and Zhang Renkai¹

¹School of Karst Science, School of Geography and Environmental Science, Guizhou Normal University, Guiyang, China, ²State Engineering Technology Institute for Karst Desertification Control, Guiyang, China, ³Anshun Agricultural Environment Field Observation and Research Station, MARA, China, ⁴School of Geographical Sciences, Southwest University, Chongqing, China

Dolomite, as a typical carbonate rock, exhibits a dual-porosity and fracture medium structure, which provides buffering systems for hydrogeochemical processes while forming unique material migration pathways. To reveal the chemical evolution patterns of karst spring water, this study collected long-term main ion chemical characteristics of karst spring water and comprehensively applied methods such as the Piper trilinear diagram, Gibbs model, ion ratios, and factor analysis to identify hydrochemical evolution characteristics and influencing factors in the spring catchment. The entropy-weighted water quality index (EWQI) was used for water quality assessment, and the potential risks of NO₃-N were evaluated using the human health risk assessment (HHRA) model. The results showed: (1) The spring water in the study area is dominated by HCO₃⁻ and Ca²⁺, primarily derived from dolomite dissolution, with a hydrochemical type of HCO₃-Ca·Mg. (2) The hydrochemical evolution in the study area is jointly influenced by rock weathering, cation exchange, and human activities, where Na+ and Cl- exhibit multisource characteristics, mainly from atmospheric deposition and anthropogenic activities. (3) According to the Chinese "Groundwater Quality Standard" (GB/T 14848-2017), all spring water in the study area falls within the "good to excellent" category. Additionally, Pearson correlation analysis between EWQI and selected indicators revealed that Ca²⁺, NO₃-N, and Cl⁻ are key factors controlling water quality. Health risk assessment indicated low non-carcinogenic risks for adults (male and female) and children, with adult males showing higher risks than children and adult females. This study holds significant implications for understanding hydrochemical evolution in dolomite karst areas and ensuring national water resource security and coordinated ecological-economic development in Southwest China.

KEYWORDS

hydrogeochemistry, water quality, influencing factors, karst spring, dolomite karst

1 Introduction

Karst groundwater, as a global strategic resource, supplies drinking water for approximately 25% of the world's population and plays a central role in the ecosystem services of karst systems (Peng et al., 2018; Ford and Williams, 2007). In China, the annual karst groundwater reserve reaches 203.967 billion m³, accounting for 26.2% of the total national groundwater resources. Previous studies on karst groundwater have predominantly focused on limestone catchments due to its higher dissolution rate compared to dolomite (Zhao et al., 2014) as well as the scattered distribution of dolomite. This has led to a long-term lack of systematic research on the hydrochemical evolution mechanisms of dolomite karst regions (Goldscheider, 2005). Addressing these gaps, investigating the geochemical characteristics and origins of karst groundwater, and clarifying the sources of hydrochemical components and water-rock interaction mechanisms are crucial for exploring hydrochemical evolution patterns in dolomite karst areas and establishing a universal hydrogeochemical baseline for regions like South China.

The relatively high magnesium ion content in water is a key distinguishing feature of karstic dolomite regions compared to other karst areas. Generally, the molar ratio of Mg²⁺/Ca²⁺ in dolomite regions ranges from 0.3 to 0.8, while in limestone regions it is below 0.2 (Diamond et al., 2024; Hilberg and Schneider, 2011). In southwestern China, under the influence of a humid climate, most dolomite karstic waters exhibit typical hydrochemical characteristics with low Mg²⁺ and high HCO₃⁻ concentrations (Wu et al., 2009). Notably, climatic conditions significantly regulate hydrochemical features: humid climates dilute dissolved substances, whereas arid regions show opposite patterns (Long et al., 2015). For instance, some dolomite karst regions in Africa demonstrate typical arid hydrochemical characteristics (Diamond et al., 2024). In the Dingling area of the Qaidam Basin, magnesium ion concentrations in dolomite aquifers even reach 2–3 times those of calcium ions (Zhang et al., 2019). Topographic conditions also impact hydrochemical profiles consider the calcitic Alps region in northern Germany and Austria, where substantial elevation gradients accelerate groundwater circulation, resulting in dolomite karstic waters with moderately elevated Mg2+ but low total dissolved solids (TDS) (Aquilina et al., 2003). Aquifer depth is another critical factor: water in deep retention zones (>200 m) achieves more stable hydrochemical composition due to comprehensive water-rock interaction, typically manifest as Na-HCO3 type waters, while shallow waters (≤200 m) are predominantly Ca-Mg-HCO₃ type (Gu et al., 2002; Leketa and Abiye, 2021). However, human activities can drastically alter hydrochemical characteristics—for example, mining activities may shift water chemistry from Mg-HCO3to Mg-SO4 (Leketa and Abiye, 2021) or produce HCO₃·SO₄-Mg·Ca mixed types (Li et al., 2023). Lithological variations also induce significant hydrochemical changes: limestone interbeds in dolomite formations can reduce Mg²⁺/Ca²⁺ ratios (Wang et al., 2022), while dolomite-evaporite mixed deposits generate complex hydrochemical profiles dominated by Mg²⁺, Ca²⁺, SO₄²⁻, and Cl⁻ ions (Barberá et al., 2014; Acero et al., 2015). Thus, while dolomite karst waters share fundamental hydrochemical patterns governed by dolomite dissolution, they exhibit pronounced regional variations influenced by geological structures, climatic conditions, hydrogeological features, and anthropogenic activities. This comprehensive analysis highlights the intricate interplay between geological setting and environmental factors in shaping karst hydrochemical systems (Diamond et al., 2024).

The Shibing dolomite karst landform in Guizhou, as the only karst system globally developed under tropical-subtropical climatic conditions, has been officially inscribed on the UNESCO World Heritage List as the core component of the "China Southern Karst" World Natural Heritage system (UNESCO World Heritage Committee, 2014). This Shibing karst research area exemplifies the morphological characteristics and evolutionary patterns of tropicalsubtropical dolomite karst, serving as a model region for karst landform dynamics and hydrochemical process studies (Li et al., 2012; Zhang et al., 2012). However, current research on Shibing's dolomite karst remains limited, particularly regarding the control mechanisms of its karst environment on regional hydrochemical processes. Investigating the chemical characteristics and ion sources of groundwater in this area is critical for understanding the formation and evolution of its karst landform. This study aims to analyze groundwater chemistry and quality assessment in Shibing's karst springs, conduct health risk assessment, and explore controlling factors of watershed hydrochemistry through human activities, atmospheric precipitation, and mineral dissolution. The research seeks to provide scientific basis for sustainable utilization of karst groundwater resources and elucidate the geomorphological processes of subtropical dolomite karst systems.

2 Materials and methods

2.1 Study area

The study area is located in the northeastern part of Shibing County, Qiandongnan Miao and Dong Autonomous Guizhou Province (107°52′37″E-108°28′47″E, 26°46′46″N-27°20′16″N). It lies at the transition zone of the Yunnan-Guizhou Plateau's eastern edge. The climate is subtropical monsoon humid, with an average annual temperature of 14.8 °C and a mean annual precipitation of 1,220 \pm 85 mm. The soil is predominantly lime soil, covering 68% of the county's area, mainly distributed in karst peak-cluster depressions, followed by yellow soil, concentrated in non-karst mountainous areas. Vegetation exhibits significant vertical zonation: evergreen broad-leaved forests dominate above 800 m, while karst shrub-fern communities prevail between 500 and 800 m, and secondary shrub-grass communities dominate below 500 m. The drainage system belongs to the Yuan River basin of the Yangtze River Basin, with the Wuyang River as the main water system. There are 24 karst springs with discharge rates exceeding 1 L/s in the county (Zhang, 2023). The topography is characterized by a NW-SE trending step-like distribution, with the highest point at Leigong Mountain (1728 m) and the lowest at the Wuyang River canyon (320 m), creating a relative elevation difference of 1,408 m. Typical karst features include peak-cluster valleys, sinkhole depressions, and natural stone bridges. The study area lies at the junction of the Yangtze Craton and the Jiangnan Orogenic Belt, with tectonic frameworks controlled by multi-stage tectonic movements during the Caledonian and Yanshan periods. Geologically, it is part of the continuous carbonate rock sedimentary area of the Lower

Cambrian Niuwaitang Formation to Qingxudong Formation (C1), with the core exposed by the Shibing Syncline, where the Qingxudong Formation dolomite outcrops in the syncline core, flanked by the Gaotai Formation and Shishuiwu Formation limestones.

Two springs, PS and BS, were selected as observation points in Shibing County. Both are exposed in the Upper Cambrian Lushan Formation (€₃1) dolomite strata, characterized by medium-to-finegrained dolomite, representing typical groundwater discharge points in the southeastern Guizhou dolomite karst area. The springs belong to different supply basins and have no direct hydraulic connection. PS Spring orifice is located at the front edge of an alluvial fan, covering an area of 2 m². It is surrounded by mixed evergreen and deciduous broad-leaved forests, with rapeseed and cabbage cultivated on the surrounding slopes, while rice paddies are distributed in the depressions. Cultivated land accounts for approximately 65% of the area, and woodland makes up about 30%. Vegetables are cultivated in multiple cycles per year, while rice is grown once a year. Nitrogenphosphorus-potassium compound fertilizers, as well as nitrogen fertilizers such as urea and ammonium sulfate, are the most commonly used fertilizers in the nearby cultivated land. Livestock manure such as cattle and chicken manure is also applied. As a historical drinking water source, the spring is located about 800 m from the residential area. Although the current permanent population in the village is small, it was once the main source of domestic water and agricultural irrigation for local residents. BS Spring orifice develops at the erosional basement level of the core valley in an anticline, with a water discharge area of 1 m². It receives dual recharge through karst fissures and conduits, demonstrating significant flow stability. The topographic units consist of steep gully slopes and erosion terraces. Approximately 75% of the surrounding area is cultivated with vegetables, while the rest is mainly shrubland. The vegetable varieties are primarily leafy greens and peppers. Nitrogen fertilizers, NPK compound fertilizers, and chicken manure are commonly used for vegetable cultivation. Due to the multiple cropping cycles of vegetables per year, the amount of fertilizer applied is relatively high. The spring is only 150 m from the residential area, and human activities are frequent. Historically, it has always been a primary source of domestic water and agricultural irrigation for the villagers. In recent years, a storage pool has been constructed to facilitate water collection (Figure 1).

2.2 Sampling and testing

In 2023, both springs were monitored under a systematic monthly sampling regime. One sampling point was established at each vent; the vents issue from separate, hydraulically disconnected recharge areas and are regarded as representative discharge points of their respective spring basins. A total of 24 samples were collected over the year, providing a comprehensive record of the hydrochemical signatures of the two catchments. Polyethylene plastic bottles were used for sampling. Before sampling, the bottles were thoroughly cleaned with distilled water and rinsed multiple times with the sample water to prevent contamination. On-site, the coordinates (latitude and longitude) and elevation of the sampling points were recorded. A portable multi-parameter water quality meter (DZB-718 model) was used to measure pH, water temperature, and total dissolved solids (TDS) *in situ*. After sampling, the bottle caps were sealed with film to prevent air entry. The samples were analyzed in

the laboratory of the National Engineering Research Center for Karst Desertification Control. Cations were analyzed using inductively coupled plasma optical emission spectrometry (ICP-OES), anions using ion chromatography, and nitrogen species using a flow analyzer. To ensure the accuracy and reliability of the results, the testing methods followed the recommended procedures in the Groundwater Quality Standard (GB/T 14848-2017), with regular calibration and quality control using standard solutions. The test results met the required quality standards.

2.3 Methods

Data processing and statistical analysis were conducted using Excel 2016. Pearson correlation analysis and principal component analysis were performed using SPSS 19.0. Piper trilinear diagrams, Gibbs diagrams, and ion ratio plots were created using Origin 2022. The Piper trilinear diagram was used to analyze the hydrochemical types of the spring water (Piper, 1944), while the Gibbs diagram and ion ratio analysis were employed to investigate the hydrochemical characteristics and primary ion sources.

Groundwater quality evaluation, as a critical method for identifying current pollution status, serves as the foundation for health risk assessments of groundwater. In recent years, the Water Quality Index (WQI) has been widely applied in groundwater quality studies across different regions due to its unique advantages (Liu and Zheng, 2022). However, the subjective selection of parameters in WQI can sometimes compromise the objectivity and accuracy of evaluations. To address this, the Entropy-Weighted Water Quality Index (EWQI) was developed to provide a more scientific and rational assessment of groundwater quality (Wang and Li, 2022). The entropy-weighted water quality index (EWQI) was applied for water quality assessment (Wang and Li, 2022), and the specific steps are shown in Equations 1–7 below:

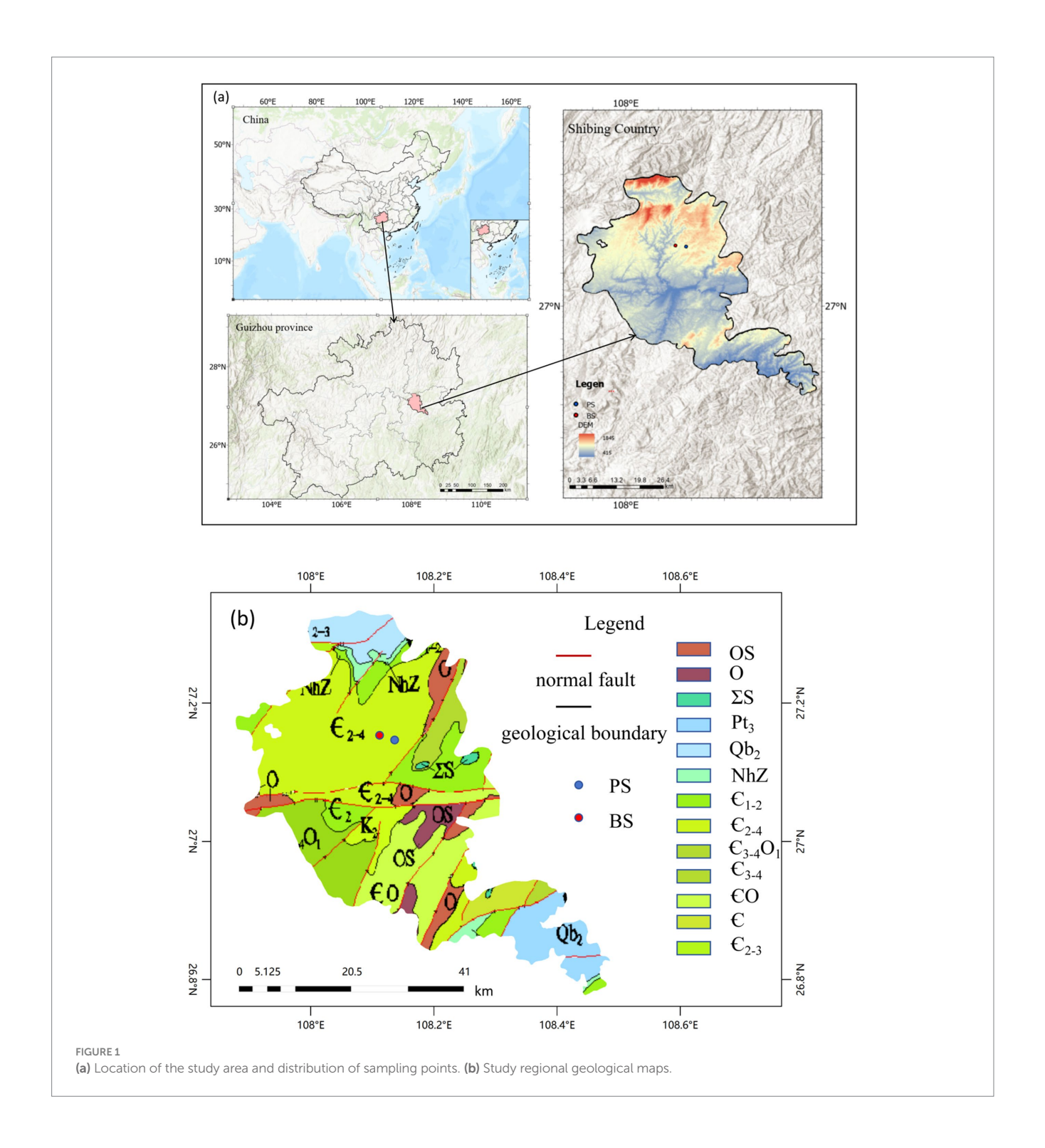
(1) Construct the characteristic matrix X for water chemistry components

$$X = \begin{bmatrix} x_{11} & x_{12} & \dots & x_{1n} \\ x_{21} & x_{22} & \dots & x_{2n} \\ \vdots & \vdots & \ddots & \vdots \\ x_{m1} & x_{m2} & \dots & x_{mn} \end{bmatrix}$$
(1)

(2) Determine the standardized parameter matrix Y

$$y_{ij} = \frac{x_{ij} - (x_{ij})_{min}}{(x_{ij})_{max} - (x_{ij})_{min}}$$
(2)

$$Y = \begin{bmatrix} y_{11} & y_{12} & \cdots & y_{1n} \\ y_{21} & y_{22} & \cdots & y_{2n} \\ \vdots & \vdots & \ddots & \vdots \\ y_{m1} & y_{m2} & \cdots & y_{mn} \end{bmatrix}$$
(3)



(3) Calculate parameter ratios P_{ij} and entropy values E_j

(4) Compute entropy weights W_j and groundwater quality classes q_i

$$P_{ij} = y_{ij} / \sum_{i=1}^{m} y_{ij}$$

$$w_{j} = 1 - E_{j} / \sum_{i=1}^{n} (1 - E_{j})$$
(6)

$$E_{j} = \frac{1}{\ln m} \times \sum_{i=1}^{m} P_{ij} \ln P_{ij}$$
 (5)
$$q_{j} = \frac{C_{j}}{S_{j}} \times 100$$

In this equation,

- m: Number of water samples.
- n: Number of selected water chemistry component parameters.
- x_{ij} : Concentration of parameter j in the i-th sample (mg L⁻¹).
- C_j: Concentration of parameter j in groundwater samples (mg L⁻¹).
- S_i: Parameter limit value (mg L⁻¹).

The EWQI classification is shown in Table 1. Generally, an EWQI value > 100 indicates water quality unsuitable for drinking.

The U.S. Environmental Protection Agency (USEPA)-developed human health risk assessment (HHRA) model was used to evaluate the potential harmful effects of groundwater pollutants on human health (Liu et al., 2022). This research considers two exposure routes: oral ingestion via drinking water and dermal absorption through direct contact. The corresponding intake calculations are shown in Equations 9–12 (Wu et al., 2020):

$$CDI_{i} = \frac{C_{i} \times IR \times ABS \times EF \times ED}{BW \times AT}$$
(9)

$$CDD_{i} = \frac{C_{i} \times SA \times KP \times EV \times ED \times CF}{BW \times AT}$$
(10)

$$HQ_{i} = \frac{CDI_{i}(CDD_{i})}{RfD}$$
 (11)

$$HI = \sum_{i=1}^{n} HQ_i \tag{12}$$

The key parameters and risk assessment criteria as follows: Parameters:

- CDI (Drinking Water Intake Dose): mg·(kg d)⁻¹.
- CDD (Dermal Contact Dose): mg·(kg d)⁻¹.
- HQ (Hazard Quotient for Non-Carcinogenic Risk): dimensionless.
- HI (Hazard Index for Total Non-Carcinogenic Risk): dimensionless.
- RfD (Reference Dose for Drinking Water Exposure): mg·(kg d)⁻¹.
- Ci (Contaminant Concentration in Groundwater): mg L⁻¹.

All other parameters are presented in Table 2 (Ministry of Ecology and Environment, 2020; Lv et al., 2025).

TABLE 1 Classification of EWQI.

EWQI range	Level	Category
EWQI < 25	1	Excellent
25 ≤ EWQI < 50	2	Good
50 ≤ EWQI < 100	3	Moderate
100 ≤ EWQI < 150	4	Poor
EWQI ≥ 150	5	Very poor

Risk Assessment Framework:

Considering physiological differences across age and gender groups, this study categorizes the local drinking water population into three groups:

- Children (0–12 years).
- Adult males (≥13 years).
- Adult females (≥13 years).

Health risk assessment is conducted separately for each demographic group. The risk classification criteria are:

- When HI/HQ < 1: The health risks caused by contamination remain within acceptable control limits.
- When HI/HQ > 1: Health risks become uncontrollable, with non-carcinogenic risks increasing proportionally with higher HI values.

3 Results

The descriptive statistical results of physicochemical indicators for PS and BS in the study area are presented in Table 3 and Figure 2. The pH values of the two karst springs ranged from 7.2 to 8.83 (mean 7.9) for PS and 7.08-8.69 (mean 7.84) for BS (Table 1), exhibiting weak alkalinity, which is related to the extensive distribution of carbonate rocks in the study area (Li et al., 2021c). The total dissolved solids (TDS) ranged from 329.8 to 650.21 mg L^{-1} (mean 453.73 mg L^{-1}) for PS and $321.3-391.1 \text{ mg L}^{-1}$ (mean 353.86 mg L^{-1}) for BS, both classified as fresh water. The TDS values at all sampling points in the spring catchment did not exceed the third-grade standard for groundwater quality (1,000 mg L⁻¹), and the coefficients of variation were all below 0.5, indicating stable TDS levels in the groundwater. Due to the slower hydrological cycle of karst spring water compared to surface or underground river water, the water-rock dissolution process was more complete, leading to higher concentrations of hydrochemical components. High concentrations of Ca²⁺ and HCO₃⁻ were the primary contributors to elevated TDS values. Notably, all karst spring samples in the study area had TDS values higher than the global average (100 mg L^{-1}) (Li et al., 2022).

The cations in the two springs are mainly Ca^{2+} and Mg^{2+} , accounting for 79.97 and 18.85% of cation concentration in PS, and 78.53 and 18.29% in BS, respectively. The concentration order was $Ca^{2+} > Mg^{2+} > K^+ > Na^+$. The anions are mainly HCO_3^- and SO_4^{2-} , accounting for 91.34 and 4.87% of anion concentration in PS, and 89.76 and 6.27% in BS, respectively. The concentration order was $HCO_3^- > SO_4^{2-} > NO_3^- > Cl^-$. The coefficients of variation for Mg^{2+} , SO_4^{2-} , and HCO_3^- were all below 0.5, indicating minimal spatial concentration variation. However, the coefficient of variation for Ca^{2+} in PS exceeded 0.5, possibly due to temporal changes in waterrock interactions.

The Piper trilinear diagram intuitively describes the composition of groundwater ions and its hydrochemical type, enabling qualitative identification of groundwater hydrochemical properties and controlling factors. In the study area, the cations of karst spring water were mainly concentrated in the Ca-type region (Figure 3), while the anions were distributed in the HCO₃⁻ type region. According to the Sukhov classification, the hydrochemical type of the spring catchment

TABLE 2 Parameters employed for human health risk assessment.

Parameter name	Abbreviation	Unit	Children	Female	Male
Drinking rate	IR	L·d ⁻¹	1.2	1.85	1.85
Average body weight	BW	kg	19.8	50	65
Exposure time	ET	h∙d ⁻¹	0.3	0.5	0.2
Gastrointestinal absorption coefficient	ABS	dimensionless	0.5	0.5	0.5
Average exposure duration	AT	d	365 × ED	365 × ED	365 × ED
Bathing frequency	EV	dimensionless	1.5	1	2
Skin permeation coefficient	KP	cm·h ^{−1}	0.001	0.001	0.001
Volume conversion factor	CF	L·cm ⁻¹	0.001	0.001	0.001
Exposure duration	ED	a	12	30	30
Exposure frequency	EF	d·a ^{−1}	365	365	365
Skin contact area	SA	cm ²	1.20E+05	1.50E+05	1.60E+05
Nitrate reference dose	RfD	mg⋅(kg⋅d) ⁻¹	1.6	1.6	1.6

was predominantly HCO_3 -Ca-Mg, indicating that the hydrochemical evolution was primarily controlled by carbonate rock dissolution. The Piper trilinear diagram showed no significant differences in hydrochemical types between PS and BS.

4 Discussion

4.1 Ion sources

4.1.1 Rock weathering

Studies on the hydrochemical characteristics of karst spring catchments based on water-rock interaction mechanisms have shown that the Gibbs model can effectively identify the dominant factors controlling groundwater formation and evolution (Yang et al., 2021). Based on TDS concentration and ion ratio characteristics, the following discriminant system can be established: Atmospheric precipitation-dominated: When TDS < 500 mg L⁻¹ and Na⁺/(Na⁺+ Ca^{2+}) > 0.3 or $Cl^-/(Cl^- + HCO_3^-)$ > 0.2. Rock weathering-dominated: When 200 mg $L^{-1} \le TDS \le 500$ mg L^{-1} and the above ratios are <0.3 and <0.2, respectively. Evaporation concentration-dominated: When TDS > 500 mg L⁻¹ and low ratios are maintained. As shown in Figure 4, the water samples from PS (TDS 329.8–650.21 mg L⁻¹, mean 453.73 mg L^{-1}) and BS (TDS $321.3-391.1 \text{ mg L}^{-1}$, mean 353.86 mg L^{-1}) were located in the rock weathering control zone of the Gibbs diagram. The Na+/(Na++ Ca2+) values ranged from 0.002 to 0.015 mg L^{-1} (PS) and $0.006-0.047 \text{ mg L}^{-1}$ (BS), while Cl⁻/ (Cl⁻ + HCO₃⁻) ranged from 0.004 to 0.007 mg L⁻¹ (PS) and 0.004-0.017 mg L⁻¹ (BS). These results confirm the dominant role of carbonate rock weathering and dissolution (Sheikhy Narany et al., 2019). All samples were far from the rainfall control zone, indicating that despite the region's high precipitation, its impact on groundwater formation was minimal. From a temporal perspective, the TDS values showed little variation, but their overall levels were high, suggesting strong water-rock interactions in the study area. PS exhibited higher TDS values than BS, possibly due to more intense rock weathering, as high concentrations of Ca2+ and HCO3- are the primary causes of elevated TDS. Currently, the springs in the study area are used for agricultural irrigation and production water. During field surveys, it was observed that local residents still perform daily activities such as washing clothes and vegetables near the springs, indicating that groundwater may be influenced by human activities in addition to water-rock interactions (Jiang et al., 2023).

The main water-rock interactions in the spring catchment are primarily the dissolution of carbonate rocks (limestone and dolomite), followed by minor dissolution of evaporite, sulfate, and silicate minerals, as well as cation exchange. To better clarify the impact of evaporite, silicate, and carbonate rock weathering on groundwater chemistry, the relationships between HCO₃⁻/Na⁺, Mg²⁺/Na⁺, and Ca²⁺/Na⁺ in each water sample were analyzed. Based on the distinct mineral compositions of different rocks, their weathering releases ions in characteristic proportions. The dissolution of evaporites typically yields very low Ca²⁺/ Na⁺ and Mg²⁺/Na⁺ molar ratios (often <0.1) due to a dominant release of Na⁺. In contrast, silicate weathering releases a more balanced suite of cations, resulting in moderate ratios (Ca²⁺/Na⁺ \approx 0.2–0.8; Mg²⁺/ $Na^+ \approx 0.1-0.6$), while carbonate dissolution, a major source of Ca^{2+} and ${\rm Mg^{2^{\scriptscriptstyle +}}}$ but not ${\rm Na^{\scriptscriptstyle +}},$ produces ratios significantly greater than 1. Therefore, these molar ratios serve as effective qualitative indicators for distinguishing the influences of evaporite, silicate, and carbonate weathering on groundwater chemistry (Gaillardet et al., 1999; Jiang et al., 2015). As shown in Figure 5, most spring samples are concentrated along the carbonate rock line and closer to the carbonate rock weathering end-member, indicating that the major ions in the study area's groundwater are primarily influenced by carbonate rock weathering. This is closely related to the widespread distribution of limestone and dolomite in the catchment. A few samples also show contributions from silicate rock dissolution. Additionally, all samples are far from the evaporite range, indicating minimal dissolution of evaporite minerals (e.g., halite, potash). As shown in Figure 5, the PS sample location is higher than BS, suggesting that PS experiences stronger carbonate rock weathering, consistent with the conclusion from the Gibbs diagram analysis.

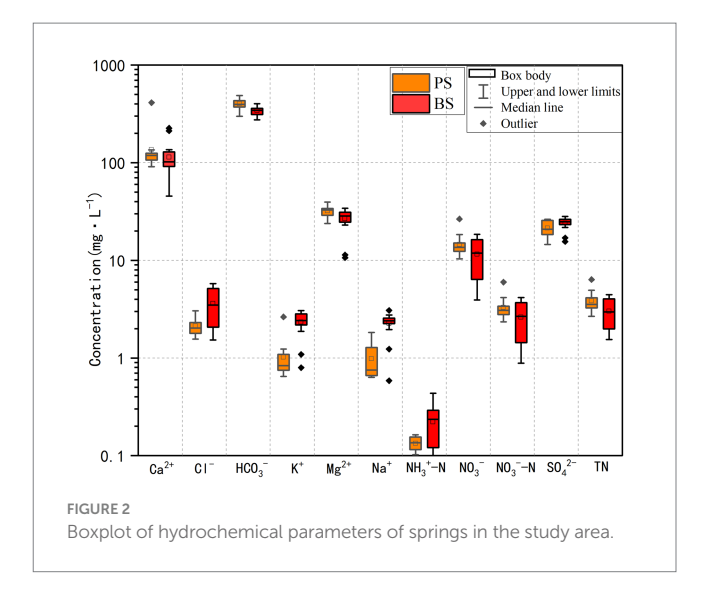
To further clarify the relative contributions of dolomite and limestone dissolution, the relationships between SO_4^{2-} and Mg^{2+}/Ca^{2+} (molar ratio) and between HCO_3^- and Mg^{2+}/Ca^{2+} (molar ratio) were analyzed. The Mg^{2+}/Ca^{2+} molar ratio can serve as an indicator of the lithology of the aquifer through which groundwater flows: values between 0.01 and 0.26 suggest flow through limestone aquifers; values >0.85 indicate flow through dolomite aquifers; and values between

4.17 2.34 5.98 0.90 3.28 0.27 0.89 1.11 2.61 mg·L 0.13 0.16 0.44 0.02 0.09 0.11 0.22 6.35 0.95 3.84 0.25 1.55 4.45 90.1 3.02 0.35 26.48 14.54 18.46 10.38 3.97 0.27 3.92 4.93 0.43 28.19 21.41 26.33 3.83 0.18 15.58 3.64 23.94 0.15 0.19 5.78 0.46 1.53 1.66 3.05 0.41 3.61 136.34 114.18 225.62 411.74 51.22 80.09 45.47 0.45 0.59 2.63 0.50 1.02 0.49 0.80 3.07 99.0 2.34 32.14 34.17 23.82 39.54 4.06 10.66 7.42 26.60 0.28 1.82 0.40 96.0 0.40 0.59 3.07 0.64 2.26 0.28 391.10 329.80 453.73 321.30 353.86 650.21 89.75 21.91 0.06 mg·L⁻ 401.73 402.60 298.90 488.00 274.50 37.39 342.91 0.12 0.11 547.65 472.00 549.50 646.80 51.35 438.00 34.39 492.27 0.09 EC ps/ cm) 0.07 7.90 7.08 8.69 0.46 8.83 0.49 90.0 7.84 90.0 H Statistics Max Max Min ME ME SD CSD S

S

BS

TABLE 3 Hydrochemical characteristics and statistical data of springs

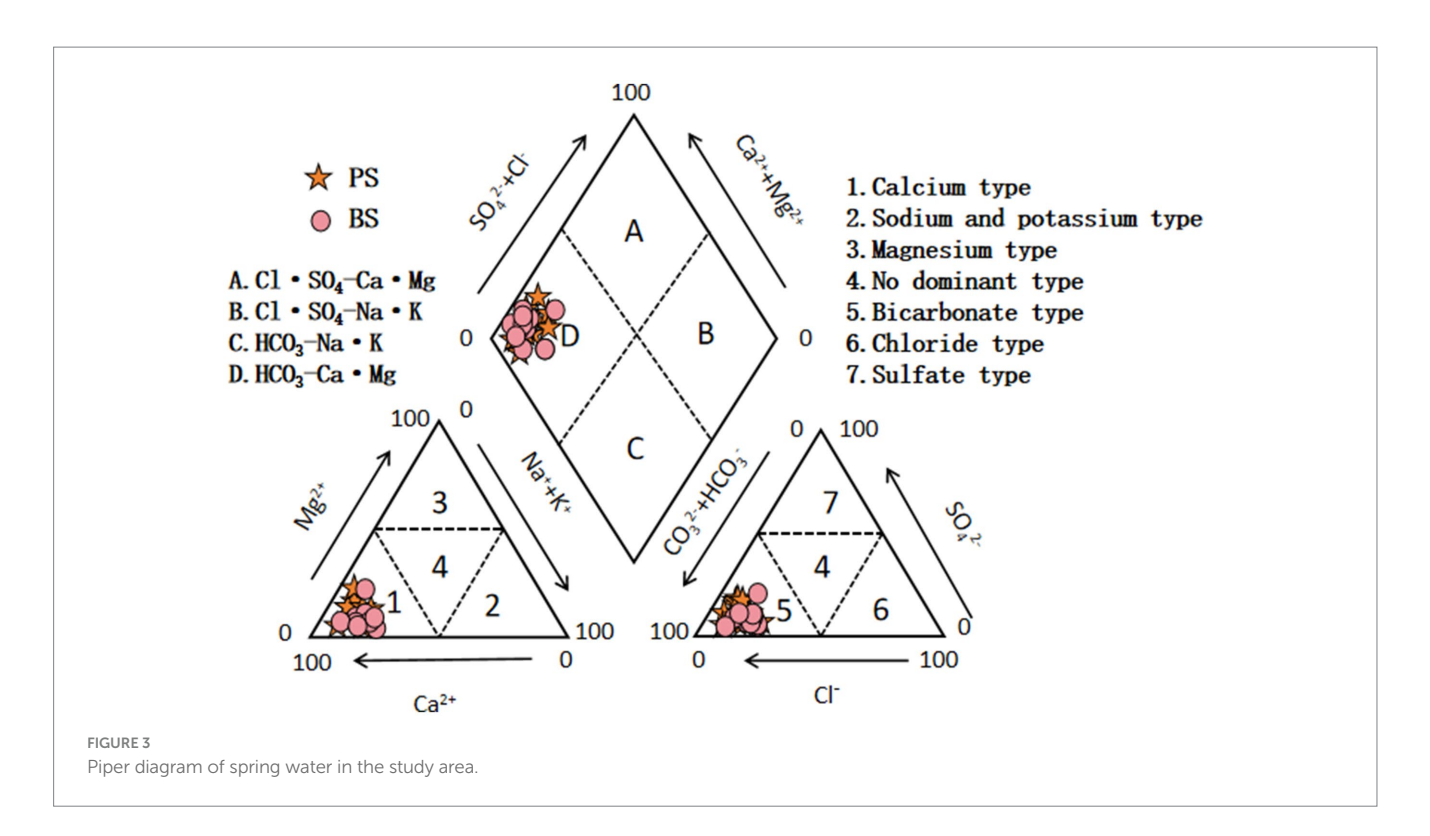


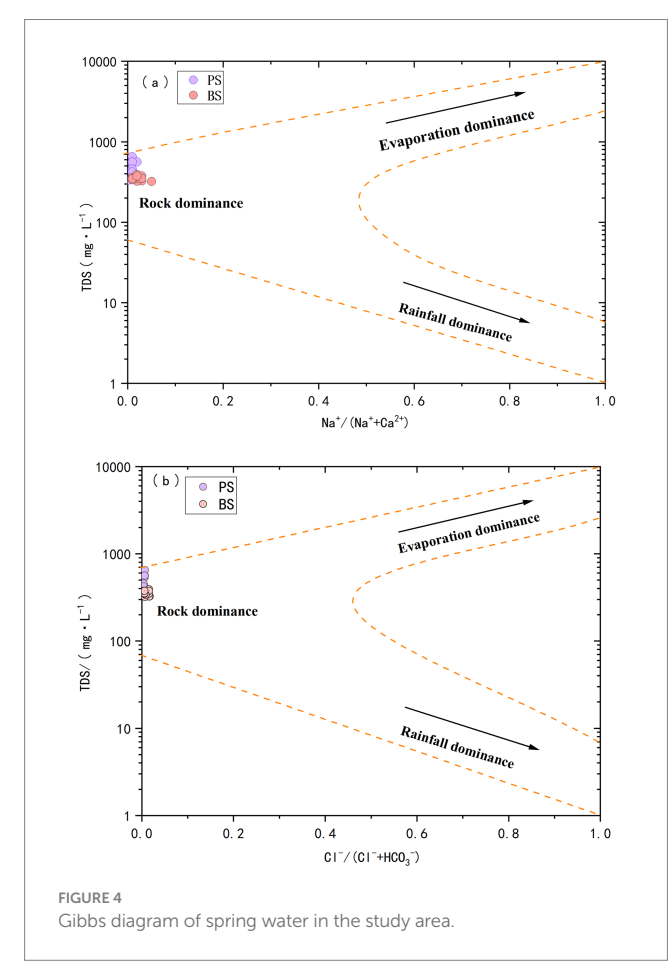
0.26 and 0.85 suggest simultaneous dissolution of both limestone and dolomite (Long et al., 2015). As shown in Figure 6, most water samples from PS and BS are primarily dominated by dissolution of both dolomite and limestone, accounting for 91.7 and 83.3% of the samples, respectively. The remaining samples are dominated by limestone dissolution alone. Although the surface geology is predominantly dolomite, the subsurface contains ancient channels, solution cave systems, or limestone interlayers (Luo et al., 2016). When groundwater flows through the dolomite layers, it may first pass through limestone regions. Additionally, the internally developed fractures in the dolomite layer could create distinct permeation pathways. Some groundwater may rapidly traverse the dolomite fractures, while other flow paths move more slowly through the limestone regions, resulting in mixing of dissolved ions from both rock types and ultimately leading to the observed combined dissolution mechanism.

Ion ratio analysis can infer hydrogeochemical processes experienced by groundwater and describe its chemical origins and identify controlling factors for chemical components (Luan et al., 2017). The relationship between HCO_3^- and $(Ca^{2+} + Mg^{2+})$ reveals the sources of Ca²⁺ and Mg²⁺. As shown in Figure 7a, both spring samples are distributed below the 1:1 line, indicating that Ca2+ and Mg2+ in the spring water mainly originate from the weathering and dissolution of carbonate minerals. To explore the balancing effect of SO₄²⁻ on cations and anions, the relationship between $(Ca^{2+} + Mg^{2+})$ and $(SO_4^{2-}/$ HCO₃⁻)was analyzed (Figure 7b), and compared with Figure 7a. The results show that the positions of the spring samples have not changed significantly, indicating that SO₄²⁻ has limited influence on the charge balance of cations and anions (Tong et al., 2021). Based on the geological conditions of the study area and human activities, it can be inferred that the aquifer types in the spring region are primarily limestone and dolomite. There are no natural sources of SO_4^{2-} such as pyrite or gypsum deposits, nor are there anthropogenic inputs like industrial discharges or wastewater effluents. As a result, the concentrations of sulfate in the spring water remain relatively low.

4.1.2 Cation exchange

 Na^+ , K^+ , and Cl^- may originate from evaporite dissolution, human activities, and cation exchange adsorption (Sae-Ju et al., 2020) and Cl^- milliequivalents can qualitatively analyze the sources of Na^+ ,





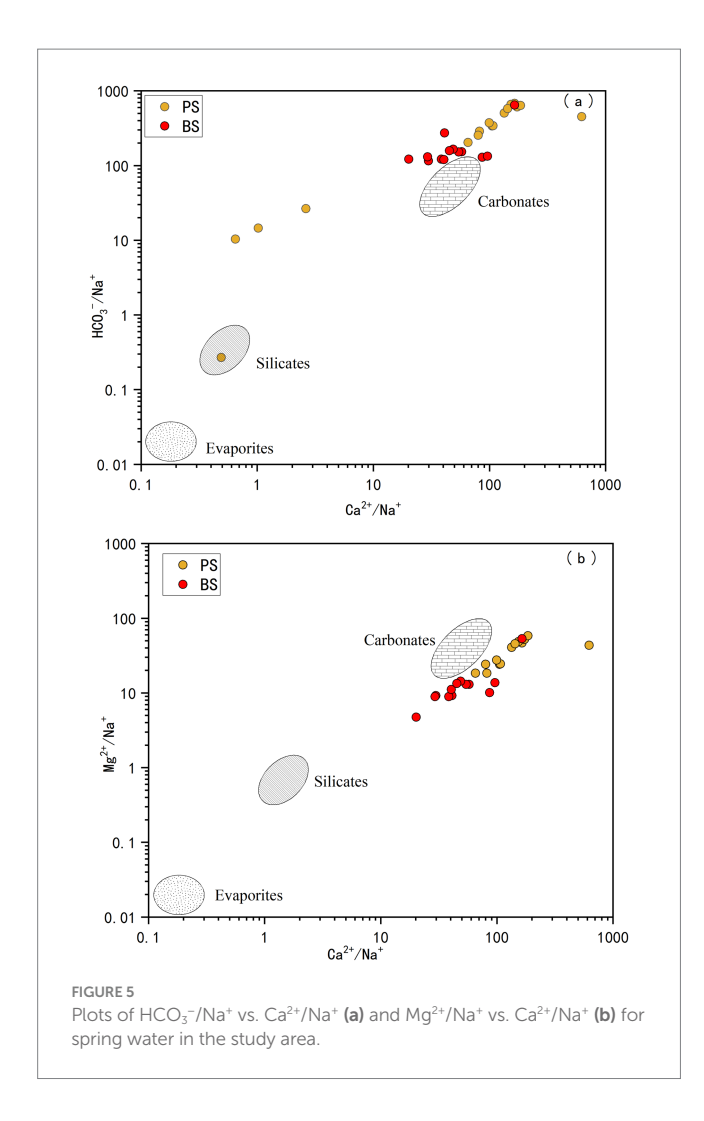
K⁺, and Cl⁻. As shown in Figure 7c, most water samples from the two springs are located near the 1:1 line, indicating consistent ion sources. Combined with the geological background of the area, where

evaporite minerals are virtually absent in the rock layers, these ions are likely derived from atmospheric deposition or human activities. However, some samples fall below the 1:1 line, suggesting that Na+ in the groundwater may also come from the dissolution of other sodium-bearing minerals (e.g., mirabilite and feldspar) or cation exchange. The Chloro-alkali Index (CAI) can further determine whether cation exchange or reverse cation exchange occurs (Schoeller, 1965). A negative CAI value indicates that Ca2+ and Mg2+ in groundwater exchange with Na+ and K+ in the aquifer rocks; a positive CAI value suggests reverse cation exchange. As shown in Figure 7d, CAI1 and CAI2 in the spring catchment are mostly negative, with some samples showing positive values, indicating that Ca2+ and Mg2+ primarily replace Na+ and K+ in the aquifer. The cation exchange process increases Na⁺ and K⁺ concentrations while decreasing Ca²⁺ and Mg²⁺ concentrations (Liu et al., 2023). Compared to PS, BS shows larger deviations from the 0 point, indicating stronger cation exchange. This aligns with Figure 7c, where BS samples are further from the 1:1 line and closer to the(Na⁺ + K⁺)axis, reflecting stronger cation exchange capacity and higher Na+ and K+ concentrations in the spring catchment.

4.1.3 Contribution ratios of major cations

The solute load in surface water and groundwater is generally influenced by rock chemical weathering, atmospheric deposition, and anthropogenic inputs. The study area in Shibing County, Guizhou Province, is primarily composed of high-purity dolomite, with almost no silicate rocks. Therefore, the solutes from rock chemical weathering in the spring water of this study area mainly originate from carbonate rocks, and silicate rocks are not considered. The following Equations 13–19 is used (Galy and France-Lanord, 1999):

$$[X]water = [X]atmospheric + [X]anthropogenic + [X]carbonate$$
 (13)



$$\begin{bmatrix} Cl^- \end{bmatrix}$$
 water = $\begin{bmatrix} Cl^- \end{bmatrix}$ atmospheric + $\begin{bmatrix} Cl^- \end{bmatrix}$ anthropogenic (14)

$$\left[\text{Cl}^{-}\right]$$
 anthropogenic = $\left[\text{Na}^{+}\right]$ anthropogenic (15)

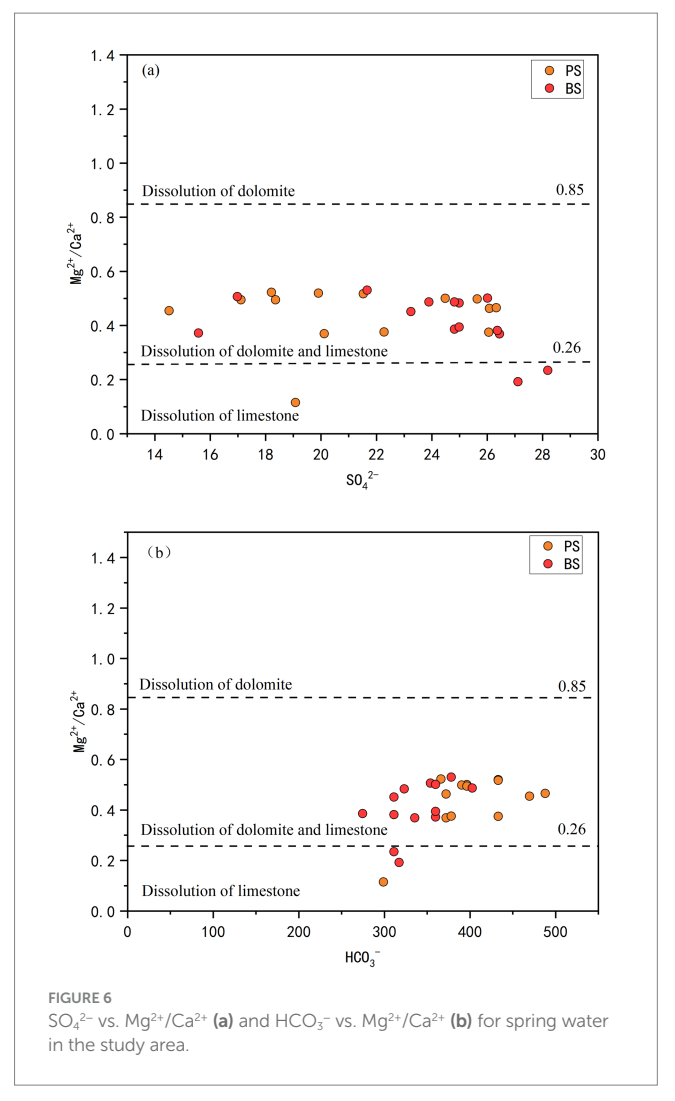
$$\begin{bmatrix} Na^{+} \end{bmatrix} water = \begin{bmatrix} Na^{+} \end{bmatrix} _{-} atmospheric + \\ \begin{bmatrix} Na^{+} \end{bmatrix} _{-} anthropogenic$$
 (16)

$$[K^{+}]$$
 water = $[K^{+}]$ atmospheric $[K^{+}]$ anthropogenic (17)

$$[Mg^{2+}]$$
 water = $[Mg^{2+}]$ atmospheric + $[Mg^{2+}]$ carbonate (18)

$$\left[Ca^{2+}\right]$$
 water = $\left[Ca^{2+}\right]$ atmospheric + $\left[Ca^{2+}\right]$ carbonate (19)

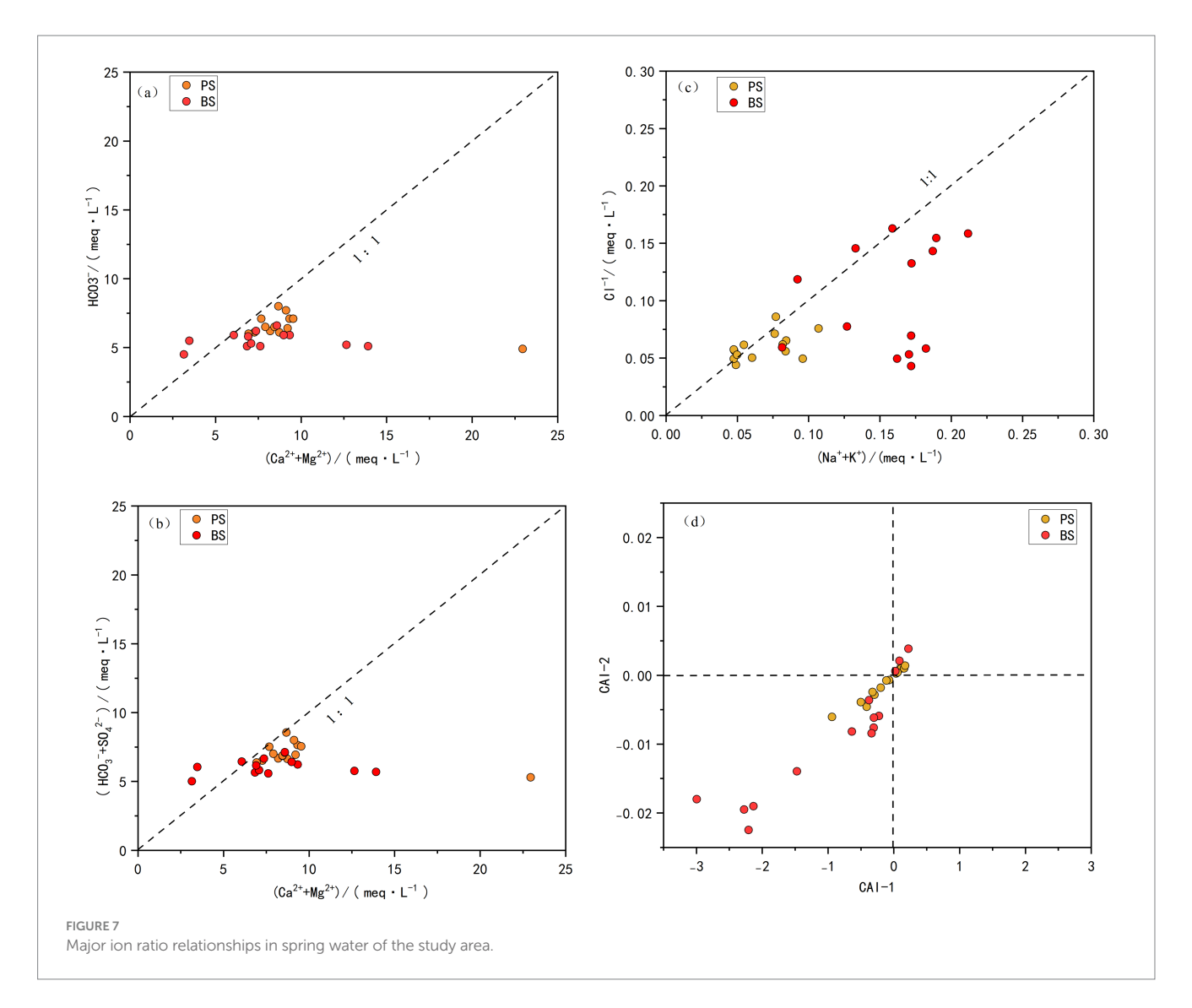
Where [X] *water* represents the ion concentration in mmol/L, [X] atmospheric denotes the atmospheric input flux, [X] anthropogenic represents the anthropogenic input flux, and [X] carbonate weathering indicates the carbonate weathering flux. The following assumptions must be satisfied during the calculation: All Cl⁻ in river water



originates entirely from atmospheric and anthropogenic inputs. After considering atmospheric input, human activities maintain a balance between Na $^+$ and Cl $^-$. There are no anthropogenic inputs of Ca $^{2+}$, and Mg $^{2+}$.

Chloride (Cl⁻) has relatively stable geochemical properties and is unaffected by physical, chemical, or microbial processes. Therefore, chloride is the most useful reference for evaluating atmospheric inputs to groundwater and surface water. To determine the atmospheric input of Cl⁻ in the study area, the annual average Cl⁻ concentration in rainfall collected from the watershed is multiplied by the evapotranspiration factor. The average rainfall and evaporation in this region are 1,033 mm and 780 mm, respectively, resulting in an evapotranspiration coefficient of 1.3. The volume-weighted average Cl⁻ concentration in rainfall in Shibing County is 1.04 mg/L, so the estimated atmospheric Cl⁻ contribution is approximately 1.33 mg/L. This calculated atmospheric input may represent the minimum contribution to river solutes.

To estimate the atmospheric input of major ions, the ratios of ions in rainfall normalized by chloride (Cl $^-$) were corrected. The calculated K $^+$ /Cl $^-$, Na $^+$ /Cl $^-$, Ca $^{2+}$ /Cl $^-$, and Mg $^{2+}$ /Cl $^-$ ratios in Shibing County rainfall are 0.19, 0.1, 0.77, and 0.08, respectively. Based on these ratios, the atmospheric contribution to spring water is relatively low for Na $^+$ and Mg $^{2+}$ (both below 5%), significant for K $^+$ (average 10.5%), and

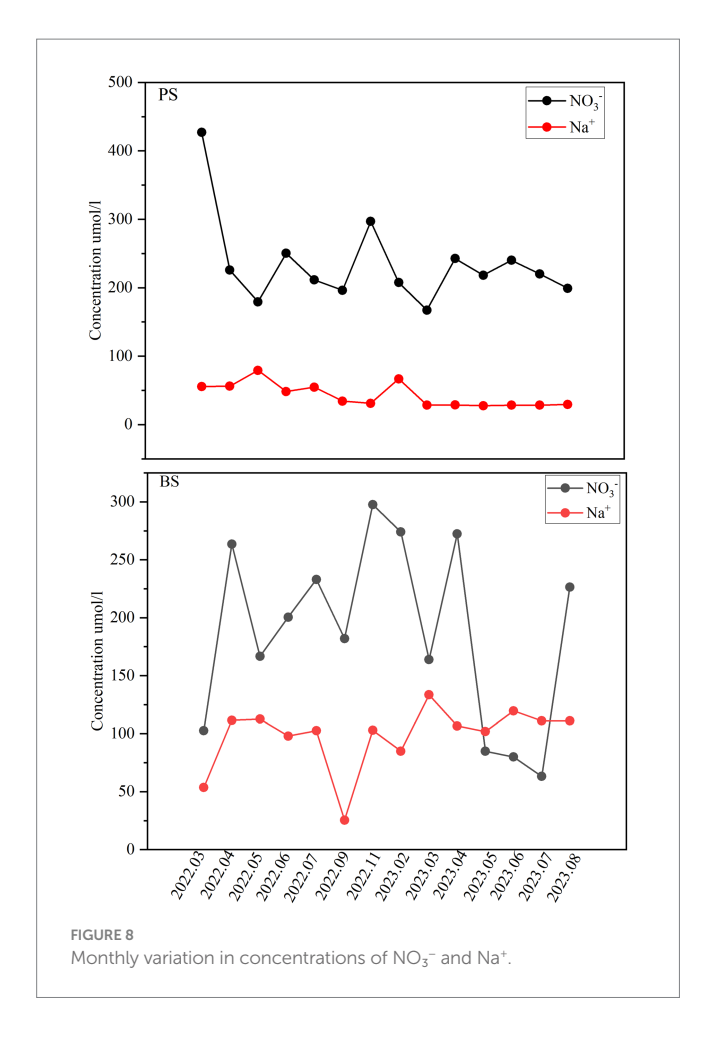


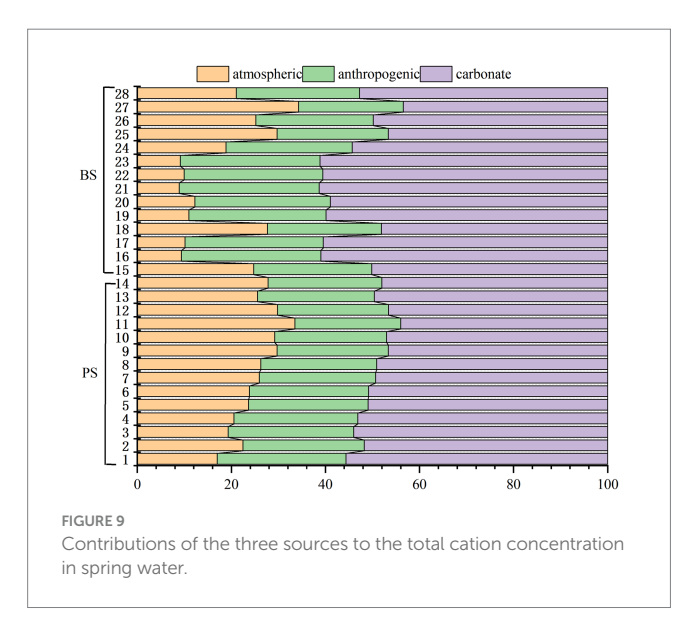
particularly high for Ca²⁺ (average 42.7%). Human activities may have a significant impact on water chemistry. The NO₃-/Na⁺ molar ratio in these waters is very high (average 4.2), far exceeding that of most springs globally. Additionally, Cl⁻ and NO₃⁻ exhibit similar trends (Figure 8), indicating a common source such as fertilizers and sewage. Furthermore, no salt-bearing strata have been found in Shibing County. Therefore, the excess Cl- after atmospheric correction can be attributed to human activities and is balanced by Na+. Thus, it is estimated that 69.5% of Na+ in the spring water originates from anthropogenic inputs. Anthropogenic inputs of Ca²⁺ and Mg²⁺ are not considered in this study. After correcting for precipitation and anthropogenic inputs, the atmospheric contributions to Ca2+ and Mg2+ are subtracted from their total concentrations, and the carbonate rock weathering contributions are estimated (as shown in the Figure 9). Overall, carbonate rock weathering contributed an average of 52.3% to the cation loading of the two spring waters, indicating that cation inputs in these springs are predominantly dominated by carbonate rock weathering. This conclusion aligns with previous studies in karst areas (Wu et al., 2025; Han et al., 2010). Notably, there were no significant differences in the contribution rates of carbonate rock weathering between the two spring waters. The atmospheric source end member accounted for an average of 21.67% of the spring water cations. By comparing the element equivalent ratios (K+/

 $Na^{+} = 0.022$, $Cl^{-}/Na^{+} = 1.17$, $Ca^{2+}/Na^{+} = 0.044$, $Mg^{2+}/Na^{+} = 0.227$, $SO_{4}^{2-}/Na^{+} = 0.022$ Na⁺ = 0.121) (Keene et al., 1986) in seawater with the rainfall-weighted average equivalent concentration ratios of ions in precipitation from Guizhou Puding (Wu et al., 2011), it was observed that, aside from longrange atmospheric transport of sea salt materials, anthropogenic inputs through atmospheric deposition significantly influenced solute concentrations in the rivers (Xu et al., 2018). The anthropogenic source end member contributed an average of 26.01% to the spring water cations, primarily driven by industrial and agricultural activities. In small catchments of coal-producing karst areas, industrial activities such as coal mining and coal washing plants have significantly elevated specific cation concentrations in water, occasionally becoming dominant input sources (Zhang et al., 2015). Generally, agricultural activities not only directly input cations into karst water systems but also indirectly affect cation balance through practices like fertilizer application, which increases nitrate (NO₃⁻) concentrations in water.

4.2 Hydrochemical control factors

Based on hydro-rock interaction and hydrogeochemical process studies, combined with correlation and factor analyses, the controlling





factors of groundwater chemistry can be effectively interpreted (Cui et al., 2020; Wang et al., 2024). Fourteen hydrochemical indicators including pH, TDS, EC, Na $^+$, K $^+$, Ca $^{2+}$, Mg $^{2+}$, HCO $_3^-$, SO $_4^{2-}$, Cl $^-$, NO $_3^-$, TN, NH $_3$ -N and NO $_3$ -N were selected for Pearson correlation analysis and factor analysis of PS and BS spring waters. The KMO and Bartlett's sphericity test results (significance level approaching zero) confirmed

the suitability of the parameters for factor analysis. As shown in Table 4, four principal components were extracted from PS samples, explaining 81.626% of the total variance, while four components were extracted from BS samples, explaining 81.993% of the variance, collectively representing the majority of hydrochemical information.

For PS, F1 emerged as the dominant hydrochemical controller, accounting for 35.21% cumulative variance (eigenvalue = 4.93). This factor exhibited strong positive loadings from Cl⁻ (0.891), Na⁺ (0.544), SO_4^{2-} (0.575), NO_3^{-} (0.778) and TN (0.878), indicating a composite hydrochemical regime influenced by anthropogenic nitrogen dynamics and chloride mobilization. The pronounced NO₃-N (r = 0.68) and TN (r = 0.878) loadings strongly suggest agricultural contamination from fertilizer leaching, corroborated by field evidence of nitrate-dominated nitrogen species (NO₃-N/TN correlation: r = 0.99). Notably, NH₃-N (loading = 0.414) showed moderate correlation with domestic sewage inputs, as evidenced by its inverse relationship with redox-sensitive parameters in F4 (NO₃loading = -0.466). F2 (eigenvalue = 3.069; cumulative variance = 57.14%) primarily reflected natural geochemical processes, characterized by HCO₃⁻ (0.789) and Mg²⁺ (0.772) loadings. This component aligns with carbonate dissolution dynamics in limestone aquifers, where groundwater-rock interaction facilitates Ca²⁺-Mg²⁺ exchange and secondary mineral precipitation (Li et al., 2021a; Zhao et al., 2021). F3 (eigenvalue = 2.056) revealed contrasting ion behavior, with Ca^{2+} showing negative loading (-0.737) and K^{+} positive loading (0.41). This pattern suggests dual control mechanisms: (1) Calcite precipitation buffering Ca2+ concentrations, and (2) preferential K+ mobilization through soil leaching, potentially mediated by cation exchange adsorption processes. F4 (eigenvalue = 1.372) displayed mixed environmental signals, with HCO₃⁻ (0.414) and SO₄²⁻ (0.457) reflecting residual dissolution processes, while negative NO₃⁻ loading (-0.466) implied transient redox perturbations possibly linked to seasonal nitrate reduction.

For BS, F1 (Eigenvalue = 4.039, cumulative variance = 28.85%) Dominated by NO_3^- (0.957), TN (0.93), and NH_3 -N (0.601), indicating nitrogen pollution primarily from agricultural activities (fertilizer leaching) and partially from domestic sewage (Gutiérrez et al., 2018; Sun et al., 2023). Figure 10 (right) shows the strong correlation (r = 0.99) between NO₃-N and TN confirms nitrate dominance in nitrogen species. In the process of agricultural production, excessive application of nitrogen fertilizer, NO₃-N and other nitrogen pollutants enter the underground aquifer through runoff or infiltration, increasing the content of NO₃-N and TN in spring water. If the domestic sewage of nearby residents is discharged directly without treatment, NH₃-N and other pollutants will enter the groundwater, which will also affect the quality of spring water (Zhang et al., 2024). F2 (Eigenvalue = 3.883, cumulative variance = 56.21%) Linked to EC (0.868), HCO₃⁻ (0.757), and TDS (0.735), suggesting mineralization processes or evaporation-driven concentration. (Eigenvalue = 1.964, variance = 70.23%) Expressed inverse relationships between K⁺ (0.915) and Ca²⁺ $(-0.56)/SO_4^{2-}$ (-0.621), possibly reflecting cation exchange or acid dissolution in soil environments. F4 (Eigenvalue = 1.646, cumulative variance = 81.99%) Involved minor (0.127) variations, likely related to localized geological heterogeneity.

In Table 4, the most prominent feature is the positive loading of pH (0.718) in the F1 factor of PS, while pH shows a significant

TABLE 4 Principal component analysis of hydrochemical components of springs.

Index	PS BS							
	F1	F2	F3	F4	F1	F2	F3	F4
рН	0.718	-0.33	0.304	-0.389	-0.751	-0.153	0.342	-0.177
EC	-0.201	0.88	0.208	-0.123	0.868	-0.033	-0.113	-0.361
HCO ₃ -	0.124	0.789	0.414	-0.31	0.757	-0.409	0.023	-0.243
TDS	0.882	-0.057	0.371	-0.084	0.735	-0.272	-0.169	-0.433
Na ⁺	0.544	-0.077	0.384	0.588	0.148	0.018	0.258	0.63
Mg ²⁺	-0.315	0.772	0.11	0.423	0.771	-0.115	0.032	0.45
K ⁺	-0.245	-0.367	0.41	-0.376	0.045	-0.047	0.915	0.26
Ca ²⁺	-0.137	-0.341	-0.737	0.203	0.288	0.059	-0.56	0.71
Cl-	0.891	0.016	0.182	0.181	0.354	0.7	0.419	-0.039
SO ₄ ²⁻	0.575	0.037	0.185	0.457	-0.548	-0.072	-0.621	0.127
NO ₃ -	0.778	0.272	-0.466	-0.264	0.18	0.957	-0.054	-0.021
TN	0.878	0.044	-0.3	0.118	0.237	0.93	-0.084	-0.045
NH ₃ -N	0.023	0.746	-0.385	-0.016	0.601	-0.595	0.116	0.214
NO ₃ -N	0.778	0.272	-0.466	-0.264	0.18	0.957	-0.054	-0.021
Eigenvalue	4.93	3.069	2.056	1.372	4.039	3.831	1.964	1.646
Contribution rate %	35.214	21.924	14.688	9.8	28.849	27.361	14.028	11.755
Cumulative contribution rate%	35.214	57.138	71.826	81.626	28.849	56.21	70.238	81.993



negative loading (-0.751) in the F1 factor of BS. Both are associated with nitrogen indicators (NO₃⁻-N, TN). This result from the factor analysis clearly reflects the fundamental difference in the degree of human activity impact they experience. The F1 of PS shows a positive correlation between pH and nitrogen (TN, NO₃⁻-N), indicating a relatively mild environment. The nitrogen primarily originates from chemical fertilizers (urea, ammonium sulfate, compound fertilizers) and manure applied to the surrounding farmland. These

nitrogen-containing substances undergo mineralization and nitrification in the soil, ultimately forming $\mathrm{NO_3}^-$ -N, which is leached into the spring water. The nitrification process produces $\mathrm{H^+}$, which should lower the pH. However, the area around PS has a considerable proportion of woodland (30%), providing a strong buffering capacity from soil organic matter and carbonate rock weathering. More importantly, the primary weathering process in the dolomite area — carbonate dissolution can consume $\mathrm{H^+}$ and produce $\mathrm{HCO_3}^-$, effectively

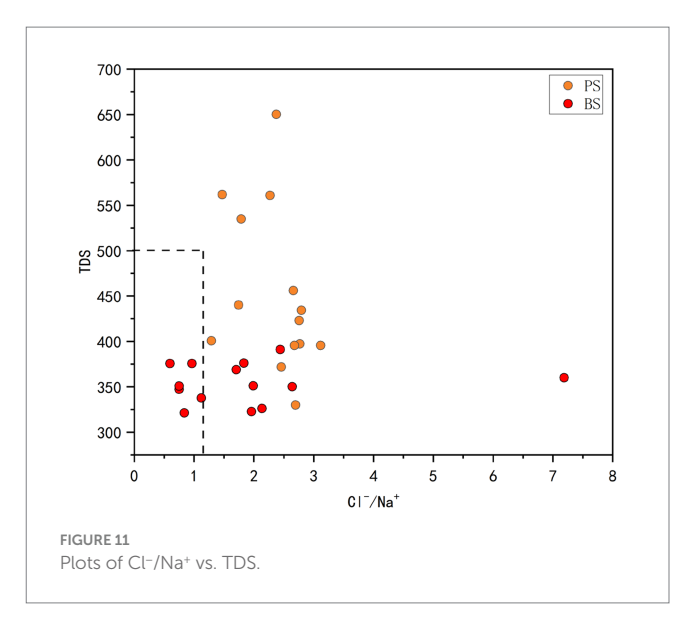
neutralizing the acidity generated by nitrification. Therefore, in PS spring, the input of nitrogen occurs simultaneously with the natural carbonate buffering system. This leads to a situation where increased nitrogen concentrations do not cause a decrease in pH; instead, a weak positive correlation emerges due to the response of the buffering system. The high loadings of TDS and Cl⁻ also support that this is a combined process of water-rock interaction and solute leaching. But the F1 of BS shows a strong negative correlation between pH and key indicators of karstification (EC, HCO₃-, Mg²⁺). This is the core "reverse characteristic." Its proximity to the residential area (only 150 m) means input of domestic wastewater (containing large amounts of organic matter and ammonium nitrogen) is a significant factor. The decomposition of organic matter and the nitrification of ammonium nitrogen both produce substantial H+, the intensity of which far exceeds that from agricultural sources in the PS area. Furthermore, the year-round multi-cropping of vegetables, with high application rates of chemical fertilizers and chicken manure, creates a continuous input of acidic substances. The acidic environment (low pH) strongly promotes the dissolution of carbonate rocks. More H⁺ reacts with HCO₃⁻, generating CO₂ and water, thereby disrupting the equilibrium and driving more Ca²⁺, Mg²⁺, and HCO₃⁻ from the rocks into the water body at a faster rate. This explains why indicators like EC, HCO₃⁻, and Mg²⁺ show a negative correlation with pH. The lower the pH, the more intense the rock dissolution, and consequently, the higher the concentration of these ions.

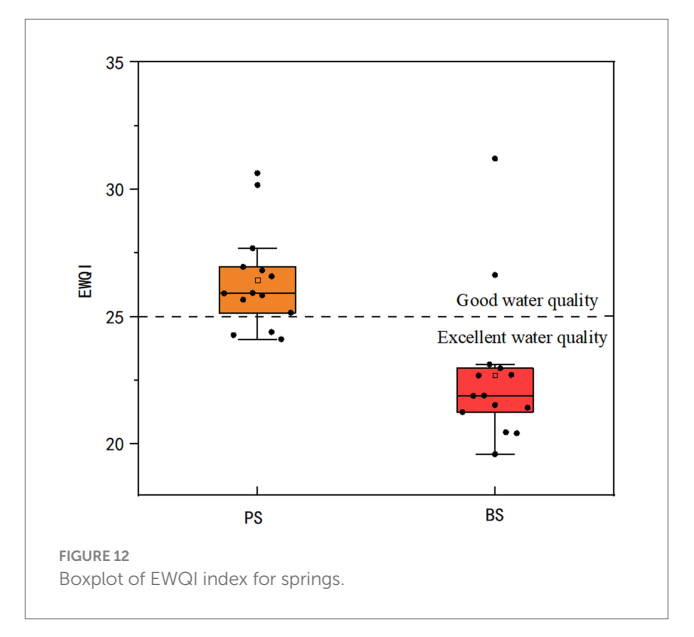
4.3 Groundwater quality assessment

Agricultural activities and unregulated discharge of domestic wastewater constrain groundwater quality and hydrogeochemical evolution, characterized by the enrichment of ions such as SO₄²⁻, Cl⁻, NO₃⁻ and Na⁺ (Yang et al., 2023; Resz et al., 2023). The sharp increase in SO₄²⁻ is primarily due to mining activities, while agricultural practices and uncontrolled discharge of domestic wastewater exacerbate the enrichment of Cl⁻, NO₃⁻, and Na⁺ (Yin et al., 2020). The ratio of TDS to Cl⁻/Na⁺ can reveal the extent of human activity impact on the watershed. When TDS $> 500 \text{ mg L}^{-1}$ or Cl⁻/Na⁺ > 1.17, it indicates significant human influence (Gaillardet et al., 1999). The TDS and Cl⁻/Na⁺ ratios in the study area's water samples are shown in Figure 11. Only a small portion of PS samples exceed 500 mg L⁻¹ TDS, while most spring samples have Cl⁻/Na⁺ ratios above 1.17. Additionally, the Cl⁻/Na⁺ ratio of PS is generally higher than that of BS, indicating that the study area's water is significantly affected by human activities.

Using 10 parameters (pH, TDS, major ions) and the Environmental Quality Index (EWQI) method based on China's Groundwater Quality Standard (GB/T 14848-2017), PS springs showed EWQI values of 24.12-30.64 (mean = 26.44), with 21.43% "excellent" (EWQI < 25) and 78.57% "good" ($25 \le EWQI < 50$) grades. BS springs exhibited superior quality (EWQI = 19.60-31.21, mean = 22.70), with 85.71% "excellent" and 14.29% "good" classifications. Both springs met direct drinking water standards (Tang et al., 2023), with BS demonstrating significantly better quality (Figure 12).

The analysis reveals distinct hydrogeochemical mechanisms governing the Environmental Water Quality Index (EWQI) (Lei et al., 2020). For PS, NO₃-N exhibits the strongest positive





correlation with EWQI (r=0.68), followed by Ca²⁺ (r=0.55) and Cl⁻ (r=0.52), collectively constituting the primary influencing factors. In contrast, the BS shows a dual-driving mechanism dominated by Ca²⁺ (r=0.59) and NO₃-N (r=0.54) as key control parameters. Notably, other ions (Mg²⁺, K⁺, SO₄²⁻, etc.) display weak correlations (r<0.4), suggesting that groundwater quality in the study area is primarily influenced by carbonate rock dissolution, with NO₃-N enrichment likely driven by anthropogenic interventions such as agricultural non-point source pollution or untreated domestic sewage discharge.

To systematically evaluate parameter contributions, a stepwise multiple linear regression model was employed, prioritizing variables based on their incremental variance contribution. The modeling process sequentially introduced predictors from highest to lowest explanatory power (Zhao et al., 2012; Song, 2012). The results are shown in Table 5: For PS, the model demonstrates that NO₃-N alone explained 47.5% of EWQI variance ($R^2 = 0.475$), with model fit increasing to 70% after incorporating Ca²⁺, and reaching 90.7% ($R^2 = 0.907$) upon adding Cl⁻.

For the BS, Ca^{2+} served as the initial dominant factor ($R^2 = 0.785$), with model explanatory power rising to 92.8% after integrating NO_3 -N and further increasing to 98.7% with Cl^- inclusion. This progressive modeling process confirms that the synergistic interaction between Ca^{2+} and NO_3 -N constitutes the core mechanism driving EWQI variations. Notably, the late-stage strong contribution of NO_3 -N suggests its potential association with temporally variable point-source pollution.

4.4 Health risk assessment

Due to the absence of sulfate minerals and heavy metal minerals near the study area, combined with the fact that the surrounding areas of the spring are predominantly agricultural land with extensive nitrogen fertilizer application, surveys revealed that nitrogen fertilizers are heavily utilized. As seen in Table 6, Correlation analyses of various indicators with EWOI (Environmental Water Quality Index) demonstrated that NO₃-N exhibited the strongest association with EWOI and NO₃-N is a key water—quality—related index (Guo et al., 2024). Since NO₃-N can harm health through drinking water intake and skin contact, causing diseases like stomach cancer and methemoglobinemia (Xie et al., 2023; Li et al., 2021b). This study focuses on its health—risk effects and Table 7 shows significant health—risk differences among exposure pathways.

The oral ingestion pathway exhibits mean Hazard Quotient (HQoral) values of 0.011 (children), 0.049 (adult females), and 0.051 (adult males), demonstrating a distinct risk gradient: adult males > adult females > children. Dermal contact risks are negligible,

with HQdermal values of 6.04×10^{-6} (children), 2.48×10^{-5} (adult females), and 1.51×10^{-5} (adult males), all well below the safety threshold (HQ = 1). Integrated Total Hazard Index (HI) assessment confirms all sampling points meet safety criteria (HI < 1). This validates the current safety of groundwater for human consumption in the study area (Tan et al., 2023; Lü et al., 2023).

It should be noted that drinking water intake is the main exposure pathway for NO₃-N related health risks, and its risk intensity is closely related to human metabolic characteristics, which is why adult men show higher sensitivity (Lv et al., 2025). Although the overall risk is currently acceptable, pollution—source management still needs strengthening. First, agricultural non—point—source pollution control should focus on regulating fertilizer and pesticide application. Second, direct pollution from laundry and vegetable—washing activities in spring—exposure areas (often in low—lying areas near homes) should be managed through environmental publicity and the establishment of protection zones. These measures are of great practical value for the sustainable use of regional groundwater resources.

5 Conclusion

(1) The spring water in the study area exhibits overall weak alkaline characteristics. The two springs show TDS concentrations ranging from 329.8 to 650.21 mg L^{-1} (mean = 453.73 mg L^{-1}) and 321.3–391.1 mg L^{-1} (mean = 353.86 mg L^{-1}), respectively, classified as freshwater. All sampling points comply with Class

TABLE 5 Stepwi	se muitipie	unear re	egression	model.
----------------	-------------	----------	-----------	--------

Spring names	Model	Linear model	R²	Р
	1	$EWQI = 21.45^2 + 0.689NO_3-N$	0.475	0.006
PS	2 EWQI = $20.001 + 0.565$ Ca ²⁺ $+0.626$ NO ₃ -N		0.79	<0.001
	3	$EWQI = 17.11 + 0.653Ca^{2+} + 0.419Cl^{-} + 0.392NO_{3}-N$	0.907	<0.001
	1	$EWQI = 18.231 + 0.886Ca^{2+}$	0.785	<0.001
BS	2	$EWQI = 14.317 + 0.844Ca^{2+} + 0.38NO_3 - N$	0.928	<0.001
	3	$EWQI = 11.615 + 0.899Ca^{2+} + 0.261Cl^{-} + 0.234NO_{3}-N$	0.987	<0.001

TABLE 6 Correlation analysis between hydrochemical components and EWQI of springs.

Pearson correlation											
Spring names	рН	TDS	Na⁺	Mg ²⁺	K ⁺	Ca ²⁺	Cl-	SO ₄ ²⁻	NH ₄ -N	NO ₃ -N	EWQI
EWQI of PS	0.138	0.394	0.205	-0.148	-0.175	0.634*	0.533*	0.272	0.268	0.689**	1
EWQI of BS	-0.129	0.083	0.056	-0.17	-0.029	0.886**	0.255	0.138	0.083	0.474	1

TABLE 7 Non-carcinogenic risk of NO₃-N under different exposure pathways.

Population		ter intake risk HQoral)	Skin contact risk index (HQdermal)		Overall ris	sk index (HI)
	Range	average	Range	average	Range	average
Children	0.003-0.022	0.011	$1.816 \times 10^{-6} \text{ to } 1.226 \times 10^{-5}$	6.042×10^{-6}	0.003-0.022	0.011
Adult female	0.015-0.099	0.049	$4.549 \times 10^{-6} \text{ to } 3.071 \times 10^{-5}$	1.514×10^{-5}	0.015-0.099	0.049
Adult male	0.015-0.104	0.051	$7.466 \times 10^{-6} \text{ to } 5.039 \times 10^{-5}$	2.484×10^{-5}	0.015-0.104	0.051

III standards of the Chinese Groundwater Quality Standard (TDS < 1,000 mg L^{-1}). Dominant ions include Ca^{2+} , Mg^{2+} , HCO_3^- , and SO_4^{2-} , with hydrochemical facies predominantly of the HCO_3 -Ca·Mg type.

- (2) The hydrogeochemical evolution is primarily controlled by rock weathering (especially dolomite dissolution in carbonate rocks), which is the main source of Ca²⁺, Mg²⁺, and HCO₃⁻ in the spring water. Cation exchange processes further modify the geochemical composition. Anthropogenic activities, including agricultural practices and domestic sewage discharge, predominantly influence Na⁺, Cl⁻ and NO₃⁻ concentrations.
- (3) In the calculation of the contribution ratios of major cations, carbonate weathering accounts for an average of 52.3% of the total cation load in the two springs, making it the dominant source. Anthropogenic inputs rank second, while atmospheric deposition contributes the least.
- (4) According to the China Groundwater Quality Standard (GB/T 14848–2017) and the EWQI classification system: the water quality samples of PS shows 21.43% in the excellent category and 78.57% in the good category. The water quality samples of BS demonstrates 85.71% in the excellent category and 14.29% in the good category. Which indicates that all spring water samples in the study area are classified within the good to excellent quality range, with BS water quality significantly outperforming PS. Regarding health risks through drinking water intake: the NO₃-N health risk index remains low, posing minimal threat to human health.
- (5) This is the first study to quantify triple-end-member solute contributions and to localize exposure parameters for HHRA in dolomite karst of South China and firstly established the control mechanisms of Mg^{2+}/Ca^{2+} in karstic dolomite spring water, providing a methodological reference for hydrochemical research in other karstic dolomite regions. However, due to limitations in investigation precision and analytical capabilities, this study lacked in-depth analysis of surface watergroundwater interactions, pollution causation mechanisms, and pollutant speciation. It also did not incorporate $\delta^{15}N$ and $\delta^{18}O$ of nitrate to quantify the contributions of fertilizers and manure. Future work should focus on these aspects to enhance the understanding of hydrological processes and pollution control strategies.

Data availability statement

The original contributions presented in the study are included in the article/supplementary material, further inquiries can be directed to the corresponding authors.

References

Acero, P., Auqué, L. F., Galve, J. P., Gutiérrez, F., Carbonel, D., Gimeno, M. J., et al. (2015). Evaluation of geochemical and hydrogeological processes by geochemical modeling in an area affected by evaporite karstification. *J. Hydrol.* 529, 1874–1889. doi: 10.1016/j.jhydrol.2015.07.028

Aquilina, L., Ladouche, B., Bakalowicz, M., et al. (2003). Deep water circulation, residence time, and chemistry in a karst complex. *Ground Water* 41, 790–805. doi: 10.1111/j.1745-6584.2003.tb02420.x

Barberá, J., Andreo, B., and Almeida, C. (2014). Using non-conservative tracers to characterise karstification processes in the Merinos-Colorado-Carrasco carbonate

Author contributions

MJ: Writing – original draft, Writing – review & editing, Methodology, Data curation. LX: Funding acquisition, Project administration, Resources, Writing – review & editing. JS: Supervision, Writing – review & editing. HJ: Project administration, Writing – review & editing. WD: Data curation, Investigation, Writing – review & editing. ZC: Investigation, Writing – review & editing. HC: Investigation, Writing – review & editing. ZR: Investigation, Writing – review & editing.

Funding

The author(s) declare that financial support was received for the research and/or publication of this article. This research was funded by the National Natural Science Foundation of China (Nos. 42301038 and 42407475), Guizhou Provincial Basic Research Program (Natural Science) (No. Yiban 1852021 Qiankehe Jichu-ZK) and Guizhou Provincial Technology Support Program (No. Yiban 2142023 Qiankehe zhicheng-ZK).

Conflict of interest

The authors declare that the research was conducted in the absence of any commercial or financial relationships that could be construed as a potential conflict of interest.

Generative AI statement

The authors declare that no Gen AI was used in the creation of this manuscript.

Any alternative text (alt text) provided alongside figures in this article has been generated by Frontiers with the support of artificial intelligence and reasonable efforts have been made to ensure accuracy, including review by the authors wherever possible. If you identify any issues, please contact us.

Publisher's note

All claims expressed in this article are solely those of the authors and do not necessarily represent those of their affiliated organizations, or those of the publisher, the editors and the reviewers. Any product that may be evaluated in this article, or claim that may be made by its manufacturer, is not guaranteed or endorsed by the publisher.

aquifer system (southern Spain). $\it Environ.~Earth~Sci.~71,~585-599.~doi: 10.1007/s12665-013-2754-8$

Cui, J. Q., Li, X. Y., Shi, H. B., et al. (2020). Chemical evolution and formation mechanism of groundwater in Hetao irrigation area. *Environ. Sci.* 41, 4011–4020. doi: 10.13227/j.hjkx.202003150

Diamond, R., van Staden, C., and Dippenaar, M. (2024). Tracing mine water flows in a dolomite quarry, South Africa, using hydrochemistry and stable isotopes. *Mine Water Environ.* 43, 278–293. doi: 10.1007/s10230-024-00980-8

- Ford, D., and Williams, P. (2007). Karst hydrogeology and geomorphology. London: Wiley, 562. doi: 10.5860/choice.45-3808
- Gaillardet, J., Dupré, B., Louvat, P., and Allègre, C. J. (1999). Global silicate weathering and CO2 consumption rates deduced from the chemistry of large rivers. *Chem. Geol.* 159, 3–30. doi: 10.1016/S0009-2541(99)00031-5
- Galy, A., and France-Lanord, C. (1999). Weathering processes in the Ganges-Brahmaputra basin and the riverine alkalinity budget. *Chem. Geol.* 159, 31–60. doi: 10.1016/S0009-2541(99)00033-9
- Goldscheider, N. (2005). Karst groundwater vulnerability mapping: application of a new method in the Swabian Alb, Germany. *Hydrogeol. J.* 13, 555–564. doi: 10.1007/s10040-003-0291-3
- Gu, J. Y., Zhang, X. Y., and Fang, H. (2002). Characteristics and genetic analysis of the deep-buried weathered-crust karst hydrocarbon reservoirs of the lower Paleozoic group in the Tarim Basin. *Acta Geol. Sin.-Engl. Ed.* 76, 494–502. doi: 10.1111/j.1755-6724.2002. tb01033.x
- Guo, H. M., Yin, J. H., Yan, S., et al. (2024). Distribution and source of nitrate in high-chromium groundwater in Jingbian, northern Shaanxi. *Earth Sci. Front.* 31, 384–399. doi: 10.13745/j.esf.sf.2024.1.24
- Gutiérrez, M., Biagioni, R. N., Alarcón-Herrera, M. T., and Rivas-Lucero, B. A. (2018). An overview of nitrate sources and operating processes in arid and semiarid aquifer systems. *Sci. Total Environ.* 624, 1513–1522. doi: 10.1016/j.scitotenv.2017.12.252
- Han, G., Tang, Y., and Xu, Z. (2010). Fluvial geochemistry of rivers draining karst terrain in Southwest China. *J. Asian Earth Sci.* 38, 65–75. doi: 10.1016/j.jseaes.2009.12.016
- Hilberg, S., and Schneider, J. F. (2011). The aquifer characteristics of the dolomite formation: a new approach for providing drinking water in the northern calcareous Alps region in Germany and Austria. *Water Resour. Manag.* 25, 2705–2729. doi: 10.1007/s11269-011-9834-x
- Jiang, L. G., Yao, Z. J., Liu, Z. F., Jiang, L., Yao, Z., Liu, Z., et al. (2015). Hydrochemistry and its controlling factors of rivers in the source region of the Yangtze River on the Tibetan plateau. *J. Geochem. Explor.* 155, 76–83. doi: 10.1016/j.gexplo.2015.04.009
- Jiang, F., Zhou, J. L., Zhou, Y. Z., et al. (2023). Hydrochemical characteristics and pollution source identification of groundwater in the plain area of the Barkol-Yiwu Basin. *Environ. Sci.* 44, 6050–6061. doi: 10.13227/j.hjkx.202211078
- Keene, W. C., Pszenny, A. A. P., Galloway, J. N., and Hawley, M. E. (1986). Sea-salt corrections and interpretation of constituent ratios in marine precipitation. *J. Geophys. Res. Atmos.* 91, 6647–6658. doi: 10.1029/JD091iD06p06647
- Lei, M., Zhou, J. L., Wu, B., et al. (2020). Hydrogeochemical evolution process of groundwater in the eastern plains in Changji hui autonomous prefecture, Xinjiang. *Arid Zone Res.* 37, 105–115. doi: 10.13866/j.azr.2020.01.12
- Leketa, K. M., and Abiye, T. A. (2021). Using environmental tracers to characterize groundwater flow mechanisms in the fractured crystalline and karst aquifers in upper crocodile river basin, Johannesburg, South Africa. *Hydrology*, 8:50. doi: 10.3390/hydrology8010050
- Li, X. Q., Hou, X. W., Wang, Z. X., Zhang, C., Ma, J., Gao, M., et al. (2023). Karst hydrogeological characteristics of Jindong large coal basin, northern China. *Environ. Earth Sci.* 82:203. doi: 10.1007/s12665-023-10869-4
- Li, X., Huang, X., and Zhang, Y. H. (2021a). Spatio-temporal analysis of groundwater chemistry, quality and potential human health risks in the Pinggu basin of North China plain: evidence from high-resolution monitoring dataset of 2015–2017. *Sci. Total Environ.* 800:149568. doi: 10.1016/j.scitotenv.2021.149568
- Li, S. Q., Xiong, K. N., Su, X. L., et al. (2012). Geomorphology and evolution of the Shibing karst site nominated for world natural heritage. *J. Guizhou Normal Univ. (Nat. Sci.)* 30, 12–17. doi: 10.16614/j.cnki.issn1004-5570.2012.03.028
- Li, J., Yang, G. L., Zhu, D. N., Yang, G., Zhu, D., Xie, H., et al. (2022). Hydrogeochemistry of karst groundwater for the environmental and health risk assessment: the case of the suburban area of Chongqing (Southwest China). *Geochemistry* 82:125866. doi: 10.1016/j.chemer.2022.125866
- Li, D. F., Zhai, Y. Z., Lei, Y., Li, D., Zhai, Y., Li, J., et al. (2021b). Spatiotemporal evolution of groundwater nitrate nitrogen levels and potential human health risks in the Songnen plain, Northeast China. *Ecotoxicol. Environ. Saf.* 208:111524. doi: 10.1016/j.ecoenv.2020.111524
- Li, J., Zou, S. Z., Zhao, Y., et al. (2021c). Major ionic characteristics and factors of karst groundwater at Huixian karst wetland, China. *Environ. Sci.* 42, 1750–1760. doi: 10.13227/j.hjkx.202009027
- Liu, M. J., Xiao, C. L., Liang, X. J., Liu, M., Xiao, C., Liang, X., et al. (2022). Response of groundwater chemical characteristics to land use types and health risk assessment of nitrate in semi-arid areas: a case study of Shuangliao City, Northeast China. *Ecotoxicol. Environ. Saf.* 236:113473. doi: 10.1016/j.ecoenv.2022.113473
- Liu, Y. L., and Zheng, Y. A. (2022). Water quality assessment and spatial-temporal variation analysis in Yellow River Basin. *Environ. Sci.* 43, 1332–1345. doi: 10.13227/j. hjkx.202106111
- Liu, Y. Q., Zhou, L., Lü, L., et al. (2023). Hydrochemical characteristics and control factors of groundwater in Shunping County, Hebei Province. *Environ. Sci.* 44, 2601–2612. doi: 10.13227/j.hikx.202205351

- Long, X., Sun, Z. Y., Liu, D. L., Sun, Z., Zhou, A., and Liu, D. (2015). Hydrogeochemical and isotopic evidence for flow paths of karst waters collected in the Heshang cave, Central China. *J. Earth Sci.* 26, 149–156. doi: 10.1007/s12583-015-0522-2
- Lü, H. Y., Dang, X. L., Zhu, Y. Y., et al. (2023). Groundwater quality analysis and health risk assessment of heavy metals in industrial areas of Henan Province, China. *J. Agro-Environ. Sci.* 42, 2740–2751. doi: 10.11654/jaes.2023-0338
- Luan, F. J., Zhou, J. L., Jia, R. L., et al. (2017). Hydrochemical characteristics and formation mechanism of groundwater in plain areas of Barkol-Yiwu Basin, Xinjiang. *Environ. Chem.* 36, 380–389. Available online at: https://kns.cnki.net/kcms2/article/abs tract?v=sUPs6kflqsYUrLfMMvbRXgU60Z_9NanSNduwGXOYQHBsJI-ewJrWRAM1I 9IB20ul3NC93kHwpn2q7aOUor0V2O1Ky2b9rsamf3STKQsb6SSIRbCbR9X1KA9kH MwVRcCCBmQWt8rm-TBJbic6QXrVgsEeNFN8wKgvQw2usJ8Yahg=&uniplatform=NZKPT
- Luo, D., Xiong, K. N., Wang, H. S., and Chen, H. (2016). Characteristics and genesis of dolomite karst caves in Shibing, Guizhou. *J. Qiannan Norm. Univ. Natl.* 36, 95–102. doi: 10.3969/j.issn.1674-2389.2016.03.023
- Lv, Y., Li, X., Yuan, J., Tian, H., Wei, T., Wang, M., et al. (2025). Hydrogeochemical Signatures and Spatiotemporal Variation of Groundwater Quality in the Upper and Lower Reaches of Rizhao Reservoir. *Water* 17:809. doi: 10.3390/w17111659
- $Ministry \ of \ Ecology \ and \ Environment \ (2020). \ Exposure factors \ handbook \ of \ Chinese \ population \ (adults). \ Beijing: \ China \ Environmental \ Press.$
- Peng, C., Pan, X. D., Jiao, Y. J., et al. (2018). Identification of nitrate pollution sources through various isotopic methods: a case study of the Huixian wetland. *Environ. Sci.* 39, 5410–5417. doi: 10.13227/j.hjkx.201803212
- Piper, A. M. (1944). A graphic procedure in the geochemical interpretation of water-analyses. EOS Trans. Am. Geophys. Union 25, 914–928. doi: 10.1029/TR025i006p00914
- Resz, M. A., Roman, C., Senila, M., et al. (2023). A comprehensive approach to the chemistry, pollution impact and risk assessment of drinking water sources in a former industrialized area of Romania. *Water* 15:1180. doi: 10.3390/w15061180
- Sae-Ju, J., Chotpantarat, S., and Thitimakorn, T. (2020). Hydrochemical, geophysical and multivariate statistical investigation of the seawater intrusion in the coastal aquifer at Phetchaburi province, Thailand. *J. Asian Earth Sci.* 191:104165. doi: 10.1016/j.jseaes.2019.104165
- Schoeller, H. (1965). "Qualitative evaluation of groundwater resources" in Methods tech. Groundw. Investig. Dev. UNESCO Water Resour. Ser, 44–52.
- Sheikhy Narany, T., Bittner, D., Disse, M., et al. (2019). Spatial and temporal variability in hydrochemistry of a small-scale dolomite karst environment. *Environ. Earth Sci.* 78:273. doi: 10.1007/s12665-019-8276-2
- Song, R. H. (2012). Application of multiple linear regression and stepwise regression in flood forecasting: a case study of the Nanting River medium- and long-term flood forecasting. *Yangtze River* 43, 122–125. doi: 10.16232/j.cnki.1001-4179.2012.s1.012
- Sun, X. B., Guo, C. L., Zhang, J., Sun, J.-q., Cui, J., and Liu, M.-h. (2023). Spatial-temporal difference between nitrate in groundwater and nitrogen in soil based on geostatistical analysis. *J. Groundwater Sci. Eng.* 11, 37–46. doi: 10.26599/JGSE.2023.9280004
- Tan, H. Y., Zhang, C. X., Li, J. S., et al. (2023). Enrichment of manganese in natural inferior groundwater and its health risk assessment in Poyang Lake Basin. *Asian J. Ecotoxicol.* 18, 227–235. doi: 10.7524/AJE.1673-5897.20220902001
- Tang, L. J., Yao, R. W., Zhang, Y. H., Tang, L., Yao, R., Zhang, Y., et al. (2023). Hydrochemical analysis and groundwater suitability for drinking and irrigation in an arid agricultural area of the Northwest China. *J. Contam. Hydrol.* 259:104256. doi: 10.1016/j.jconhyd.2023.104256
- Tong, H., Gao, Z. J., Gao, F. S., et al. (2021). Hydrochemical characteristics and water quality evaluation of groundwater in the west of Yi River basin. *Environ. Chem.* 40, 3443–3454. doi: 10.7524/j.issn.0254-6108.2020122802
- UNESCO World Heritage Committee (2014). State of conservation of the properties inscribed on the List of World Heritage in Danger (WHC-14/38.COM/7A). 38th session (Doha, Qatar: World Heritage Centre), 15–25.
- Wang, Y. H., and Li, P. Y. (2022). Appraisal of shallow groundwater quality with human health risk assessment in different seasons in rural areas of the Guanzhong plain (China). *Environ. Res.* 207:112210. doi: 10.1016/j.envres.2021.112210
- Wang, R., Li, X. H., and Wei, A. H. (2022). Hydrogeochemical characteristics and gradual changes of groundwater in the Baiquan karst spring region, northern China. *Carbonates Evaporites* 37:47. doi: 10.1007/s13146-022-00794-1
- Wang, S., Ren, Y., Guo, H., et al. (2024). Chemical characteristics of shallow groundwater in the Yellow River diversion area of Henan Province and identification of main control pollution sources. *Environ. Sci.* 45, 792–801. doi: 10.13227/j. hikx.202303263
- Wu, Q., Han, G., Tao, F., et al. (2011). Chemical composition of precipitation in a karst rural area of Southwest China: a case study in Puding, Guizhou. *Environ. Sci.* 32, 26–32. doi: 10.13227/j.hjkx.2011.01.004
- Wu, P., Tang, C. Y., Zhu, L. J., Tang, C., Zhu, L., Liu, C., et al. (2009). Hydrogeochemical characteristics of surface water and groundwater in the karst basin, Southwest China. *Hydrol. Process.* 23, 2012–2022. doi: 10.1002/hyp.7332

Wu, D., Zeng, Y., Li, P., et al. (2025). Weathering characteristics and carbon sink effect of rocks under exogenous acid action: a case study of the Chishui River. *Geol. China*, 1–26. Available online at: https://link.cnki.net/urlid/11.1167.P.20250902.1653.012

- Wu, J. H., Zhang, Y. X., and Zhou, H. (2020). Groundwater chemistry and groundwater quality index incorporating health risk weighting in Dingbian County, Ordos Basin of Northwest China. *Geochemistry* 80:125607. doi: 10.1016/j.chemer.2020.125607
- Xie, H., Zou, S. Z., Li, J., et al. (2023). Spatial distribution, source analysis, and health risk assessment of metal elements in karst water in southeastern Chongqing. *Environ. Sci.* 44, 4304–4313. doi: 10.13227/j.hjkx.202208239
- Xu, S., Li, S. L., Zhong, J., et al. (2018). Hydrochemical characteristics and rock weathering mechanisms in the Chishui River basin. *Chin. J. Ecol.* 37, 667–678. doi: 10.13292/j.1000-4890.201803.031
- Yang, F., Liu, S., Jia, C., Gao, M., Chang, W., and Wang, Y. (2021). Hydrochemical characteristics and functions of groundwater in southern Laizhou Bay based on the multivariate statistical analysis approach. *Estuar. Coast. Shelf Sci.* 250:107153. doi: 10.1016/j.ecss.2020.107153
- Yang, Y., Mei, A., Gao, S., and Zhao, D. (2023). Both natural and anthropogenic factors control surface water and groundwater chemistry and quality in the Ningtiaota coalfield of Ordos Basin, northwestern China. *Environ. Sci. Pollut. Res.* 30, 67227–67249. doi: 10.1007/s11356-023-27147-2
- Yin, C., Yang, H. Q., Wang, J. F., Yang, H., Wang, J., Guo, J., et al. (2020). Combined use of stable nitrogen and oxygen isotopes to constrain the nitrate sources in a karst lake. *Agric. Ecosyst. Environ.* 303:107089. doi: 10.1016/j.agee.2020.107089
- Zhang, R. K. (2023). Nitrogen output in the surface karst zone of rocky desertification areas and its environmental significance. Guiyang: Guizhou Normal University. doi: 10.27048/d.cnki.ggzsu.2023.001086

- Zhang, Q. Z., Liu, Z. Q., Luo, J. S., et al. (2012). Influence of petro-geochemical characteristics on the morphology and distribution of karst canyons: a case study of the Shibing karst world natural heritage candidate site, Guizhou. *J. Southw. Univ. (Nat. Sci. Ed.)* 34, 114–120. doi: 10.13718/j.cnki.xdzk.2012.06.014
- Zhang, Y., Liu, J. T., Zhou, S. Y., et al. (2024). Characteristics, controlling factors and effects on human health of groundwater chemical evolution in Wenzhou plain, lower Oujiang River catchment. *Geol. China* 51, 1059–1073. doi: 10.12029/gc202309 11002
- Zhang, D., Qin, Y., and Zhao, Z. Q. (2015). Involvement of sulfuric acid in the chemical weathering of carbonate minerals in a small catchment of northern China. *Acta Sci. Circum.* 35, 3568–3578. doi: 10.13671/j.hjkxxb.2015. 0097
- Zhang, Z. X., Xu, Y. X., Cao, J. H., Zhang, Z., Xu, Y., Zhang, Y., et al. (2019). Review: karst springs in Shanxi, China. *Carbonates Evaporites* 34, 1213–1240. doi: 10.1007/s13146-018-0440-3
- Zhao, Y., Hua, X. H., and Li, M. (2012). Application of stepwise regression model in surface subsidence monitoring. *Geomat. Inf. Sci. Wuhan Univ.* 37, 6–8+35. doi: 10.14188/j.2095-6045.2012.01.001
- Zhao, W. Z., Shen, A. J., Zheng, J. F., et al. (2014). Discussion on the origin of porosity in dolomite reservoirs in the Tarim, Sichuan, and Ordos basins and its guidance for reservoir prediction. *Sci. China Earth Sci.* 57, 2498–2511. doi: 10.1007/s11430-014-4920-6
- Zhao, W. D., Zhao, L., Gong, J. S., et al. (2021). Pollution assessment and source apportionment of shallow groundwater in Suzhou mining area, China. *Earth Sci. Front.* 28, 1–14. doi: 10.13745/j.esf.sf.2021.2.8